Measurement of plasma parameters in the far-field plume of a Hall effect thruster

2011 Plasma Sources Sci. Technol. 20 065012

(http://iopscience.iop.org/0963-0252/20/6/065012)

Plasma Sources Sci. Technol. **20** (2011) 065012 (9pp) doi:10.1088/0963-0252/20/6/065012

Measurement of plasma parameters in the far-field plume of a Hall effect thruster

K Dannenmayer[1], P Kudrna[2], M Tichý[2] and S Mazouffre[1]

[1] Institut de Combustion, Aérothermique, Réactivité et Environnement, CNRS, Orléans, France
[2] Faculty of Mathematics and Physics, Charles University, Prague, Czech Republic

E-mail: kathe.dannenmayer@cnrs-orleans.fr

Received 1 June 2011, in final form 17 October 2011
Published 29 November 2011
Online at stacks.iop.org/PSST/20/065012

Abstract
The far-field plume of a 1.5 kW Hall effect thruster is mapped with a Langmuir probe and an emissive probe. Time-averaged measurements of the plasma potential, the electron temperature and the electron number density are performed for different operating conditions of the thruster. The influence of the discharge voltage, the cathode mass flow rate as well as the magnetic field strength is investigated. The plasma potential decreases from 30 V at 300 mm on the thruster axis to 5 V at 660 mm and at 60°, the electron temperature decreases from 5 to 1.5 eV. The electron number density drops from 3.5×10^{16} to 1×10^{15} m^{-3} in the far-field plume. The values of the plasma potential and electron temperature measured with the Langmuir probe and the emissive probe are in good agreement.

(Some figures may appear in colour only in the online journal)

1. Introduction

Crossed field discharges are often used in the field of plasma physics, for example in Hall effect thrusters (HETs) used as space propulsion devices [1], in magnetized plasma columns for fundamental studies of turbulence and instabilities [2], in end-Hall ion sources for plasma processing and coating formation [3, 4], in the edge and the divertor region of a tokamak reactor [5] and in the magnetic filter region of a negative ion source for neutral beam generation [6, 7]. This work is focused on HETs.

Electric propulsion is at present a well-established technology for space applications [8]. In comparison with chemical rocket jets, electric propulsion devices offer an attractive way to save propellant mass thanks to a much faster propellant ejection speed. Among all electric propulsion devices, HETs are currently recognized as an attractive propulsion means for long duration missions and maneuvers that require a large velocity increment. They are used for geosynchronous satellite attitude control and station keeping [1, 9]. As demonstrated by the successful SMART-1 moon mission, HETs can also be used as primary propulsion engines for orbit transfer maneuvers [10].

The basic physics of a Hall thruster consists of a magnetic barrier in a low-pressure dc discharge maintained between an external cathode and an anode [1, 9]. The anode, which also serves as the gas injector, is located at the upstream end of a coaxial annular dielectric channel that confines the discharge. Xenon is generally used as the working gas for its specific properties in terms of atomic mass and low ionization energy. A set of solenoids provides a radially directed magnetic field whose strength is maximum in the vicinity of the channel exit. The magnetic field is chosen strong enough to make the electron Larmor radius much smaller than the discharge chamber sizes, but weak enough not to affect ion trajectories. The electric potential drop is mostly concentrated in the final section of the channel owing to the high electron resistivity. The corresponding local axial electric field drives a high azimuthal drift—the Hall current—that is responsible for the efficient ionization of the supplied gas. It also accelerates ions out of the channel, which generates thrust. The ion beam is neutralized by a fraction of electrons emitted from the cathode.

The plasma plume of HETs exhibits a relatively large divergence angle of about 45° [11]. Although the plume is quasineutral, it still consists of charged particles, which leads to electrical and mechanical interactions with the spacecraft [12]. It is thus important to develop and improve models of the plume in order to help in assessing the spacecraft integration issues. The numerical models of the thruster plume need to be validated by comparison with experimental data. Therefore

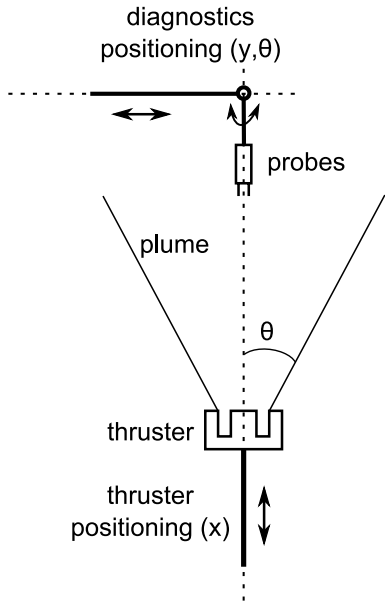

Figure 1. Schematic view of the Hall thruster and probe positioning system.

the entire plasma plume needs to be mapped to obtain ion, electron and neutral properties.

The global dynamic of the discharge is controlled by the electrons. The presented experimental investigations focus thus on the electron properties in the far-field plume of a HET. The plasma potential V_p, the electron temperature T_e and the electron number density n_e are measured with a Langmuir probe (LP) and an emissive probe (EP) for different operating conditions of the 1.5 kW-class PPS100-ML thruster. The far-field plume is mapped between 300 and 660 mm downstream the thruster exit plane and between 0° and 60°, where 0° corresponds to the thruster axis. The influence of the discharge voltage U_d, the cathode mass flow rate $\dot{m}_c$ as well as the magnetic field strength is investigated by time-averaged measurements. Plasma potential and electron temperature values obtained with both types of probes are compared.

2. Experimental set-up

The experimental work was carried out in the plume of a laboratory HET, operating in the ground-test facility PIVOINE-2g in Orléans, France [13]. The thruster is mounted on a moveable arm that allows the displacement of the thruster along the thrust axis (x-direction). The diagnostics are mounted on a second arm that moves perpendicular to the thrust axis (y-direction). A rotation stage at the end of the diagnostics arm allows the displacement of the probes in the θ-direction, so that the probes always point toward the thruster center. The combination of the displacements of the probes in the y- and θ-directions together with the possibility to move the thruster along its axis allows mapping of the complete far-field plume, see figure 1.

For the experiments a PPS100-ML thruster was used. The PPS100-ML is a 1.5 kW HET with a discharge chamber outer diameter of 100 mm [14]. The channel walls were made of $BNSiO_2$. In this study, the original version with coils and a version with permanent magnets were used [15]. The magnetic field topology with permanent magnets was roughly the same as for the original version with a coil current of 4.5 A. The magnetic field was maximum in the thruster exit plane and it decreased rapidly outside the discharge chamber. In the far-field plume the magnetic field strength was below 1 G and the plasma could therefore be considered as magnetic field free. The thruster was equipped with a heated cathode provided by MIREA [16]. The thruster parameters, e.g. discharge current and cathode potential versus ground, were constantly recorded.

A single cylindrical LP was used to characterize the far-field plume of the PPS100-ML. The LP was made of a tungsten wire 0.38 mm in diameter. The non-collecting part of the wire was insulated from the plasma by a 100 mm long and 2 mm diameter alumina tube. The length of the collecting part was 5 mm. The voltage sweep and the resulting probe current measurement were performed using the ALP System™ manufactured by Impedans. The parameters V_p, T_e and n_e were derived from the probe characteristics using the standard Langmuir probe theory in a collisionless and magnetic field free plasma assuming a Maxwellian electron distribution function [17, 18]. The plasma potential is obtained from the maximum of the first derivative of the probe characteristic ($V_p = (\mathrm{d}I/\mathrm{d}V)_{max}$); it can also be obtained from the intersection of linear fits in the transition and electron saturation regions. The electron temperature is determined from the slope of the logarithm of the electron current in the transition region ($T_e = (\frac{\mathrm{d}\ln I_e}{\mathrm{d}V})^{-1}$). The electron density is calculated using the orbital motion limited (OML) assumption; in the OML regime the slope of I_e^2 versus V plot is proportional to n_e^2. An example of the current–voltage characteristics and the resulting analysis is given in figure 2.

The plasma potential was also measured using a floating EP. The emitting part of the probe consisted of an 8 mm long loop of a thoriated tungsten wire of diameter 150 μm. The ends of the wire were mechanically crimped to copper wires and inserted into two parallel holes of a 100 mm long and 4 mm diameter alumina tube. The filament was heated with a dc power supply up to the regime of electron emission. In the ideal case the floating potential of a sufficiently emitting probe is equal to the plasma potential. In this case the electron current is completely compensated by the emission current from the probe, therefore no net current flows through the probe and there is no sheath around the probe [19]. However the electrons emitted by the probe are usually colder than the electrons in the plasma. The space charge of the cold emitted electrons causes a saturation of the sheath around the hot filament and therefore the measured probe potential is not exactly equal to the plasma potential [20]. If the temperature of the plasma electrons is large compared with the temperature of the emitted electrons, the plasma potential measured with the EP is underestimated. If the emitted electrons and the plasma electrons have approximately the same temperature, the value of the plasma potential measured by the EP is overestimated. The electron temperature can also be determined from the EP measurements. The probe floating potential has to be recorded for the cold probe as well as for the sufficiently heated

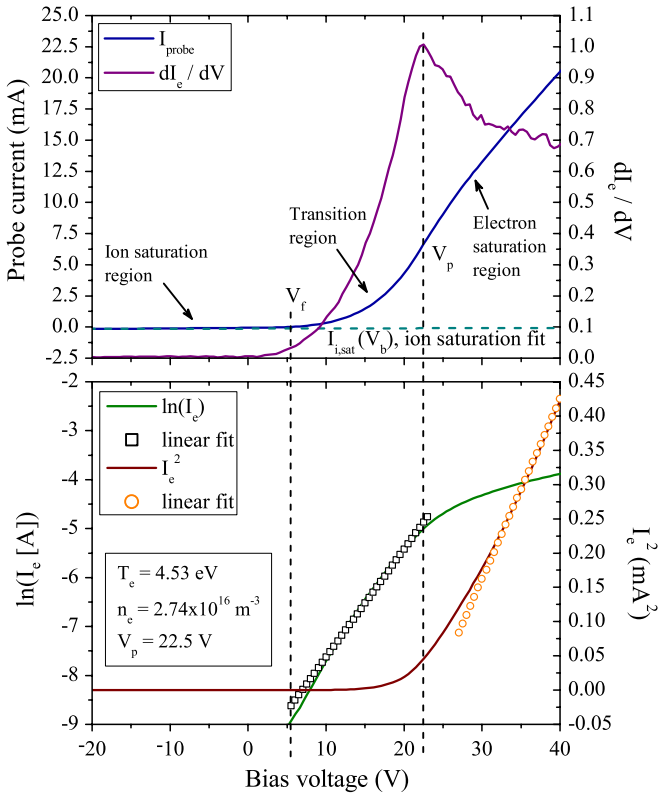

Figure 2. Example of current–voltage characteristics recorded at a discharge voltage of 200 V and a mass flow rate of 4.0 mg s^{-1}.

probe. The electron temperature can then be determined using an adequate model of the collected electron and ion current [21, 22]. A typical measurement of the probe potential as a function of the heating current is depicted in figure 3. As can be seen in figure 3, the probe potential never really saturates but the slope clearly levels off if the current is increased above 4 A. This has already been observed in other thrusters and plasma sources [20, 23]. For the measurement of the plasma potential in the far-field, the heating current was fixed to 4.5 A. The lifetime of the EP in the far-field was in the order of several hours allowing a complete mapping of the far-field with one probe.

The probes are mounted next to each other. The probe axis is parallel to the thruster axis. An examination of the discharge current evolution for different probe positions reveals that the probes do not influence the discharge behavior.

3. Results

The measurement of the plasma parameters in the far-field plume of the PPS100-ML is presented for different operating conditions of the thruster. The discharge voltage, the cathode mass flow rate and the coil current are varied in order to check their influence on V_p, T_e and n_e. For every operating condition the discharge current oscillations and the cathode potential towards ground are recorded. A comparison of the discharge current and the discharge current oscillations for different probe positions in the plume reveals no influence of the probes on the discharge behavior regardless of their position.

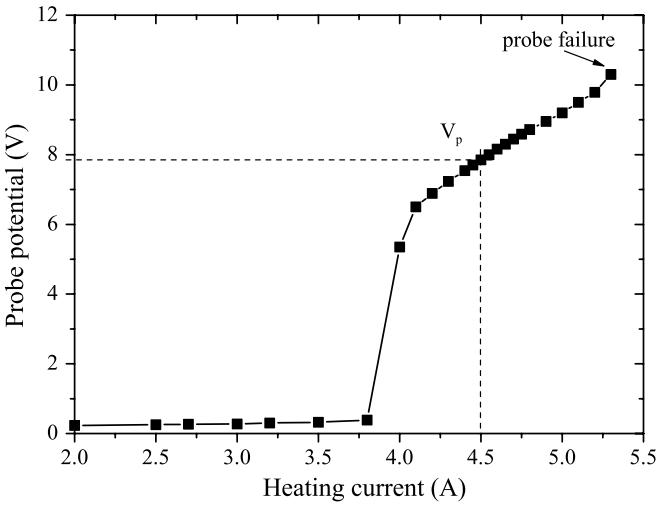

Figure 3. EP potential against the heating current in the far-field plume of the PPS100-ML thruster.

The measurements with the LP and the EP were carried out simultaneously after verification that the two measurements do not influence each other.

3.1. Complete map

An example for a complete map of the far-field plume between 300 and 660 mm and from 0° to 60° measured with a LP is shown in figure 4. The PPS100-ML is fired at a discharge voltage of $U_d = 300$ V, an anode mass flow rate of $\dot{m}_a = 4.0$ mg s^{-1} and a cathode mass flow rate of $\dot{m}_c = 0.42$ mg s^{-1}. The magnetic field is provided by permanent magnets.

3.2. Influence of the discharge voltage

The influence of the discharge voltage on the plasma parameters is investigated at constant anode and cathode mass flow rates ($\dot{m}_a = 4.0$ mg s^{-1} and $\dot{m}_c = 0.42$ mg s^{-1}). The magnetic field is again provided by permanent magnets. Figure 5 shows the variation of V_p, T_e and n_e measured with an LP as a function of the angle θ for three different discharge voltages. For the sake of clarity the results are presented only for two different distances from the thruster exit plane, 300 mm and 500 mm, respectively.

The cathode potential to ground is very similar for the three operating conditions: $V_c = 14 \pm 1$ V, see table 1. As can be seen from table 1, the mean discharge current is almost the same for a discharge voltage of 150 and 200 V; the current standard deviation is higher for $U_d = 150$ V. For $U_d = 300$ V the mean discharge current and the current standard deviation are highest.

As can be seen in figure 5(*a*), the plasma potential V_p decreases with the angle θ. For angles smaller than 20° the plasma potential is higher for a higher discharge voltage. For $\theta > 20°$, there is no clear difference for the three different operating conditions. The electron temperature T_e also decreases with the angle θ, as shown in figure 5(*b*). For $\theta < 30°$, the electron temperature is higher for a higher discharge voltage, whereas for $\theta > 30°$, there is

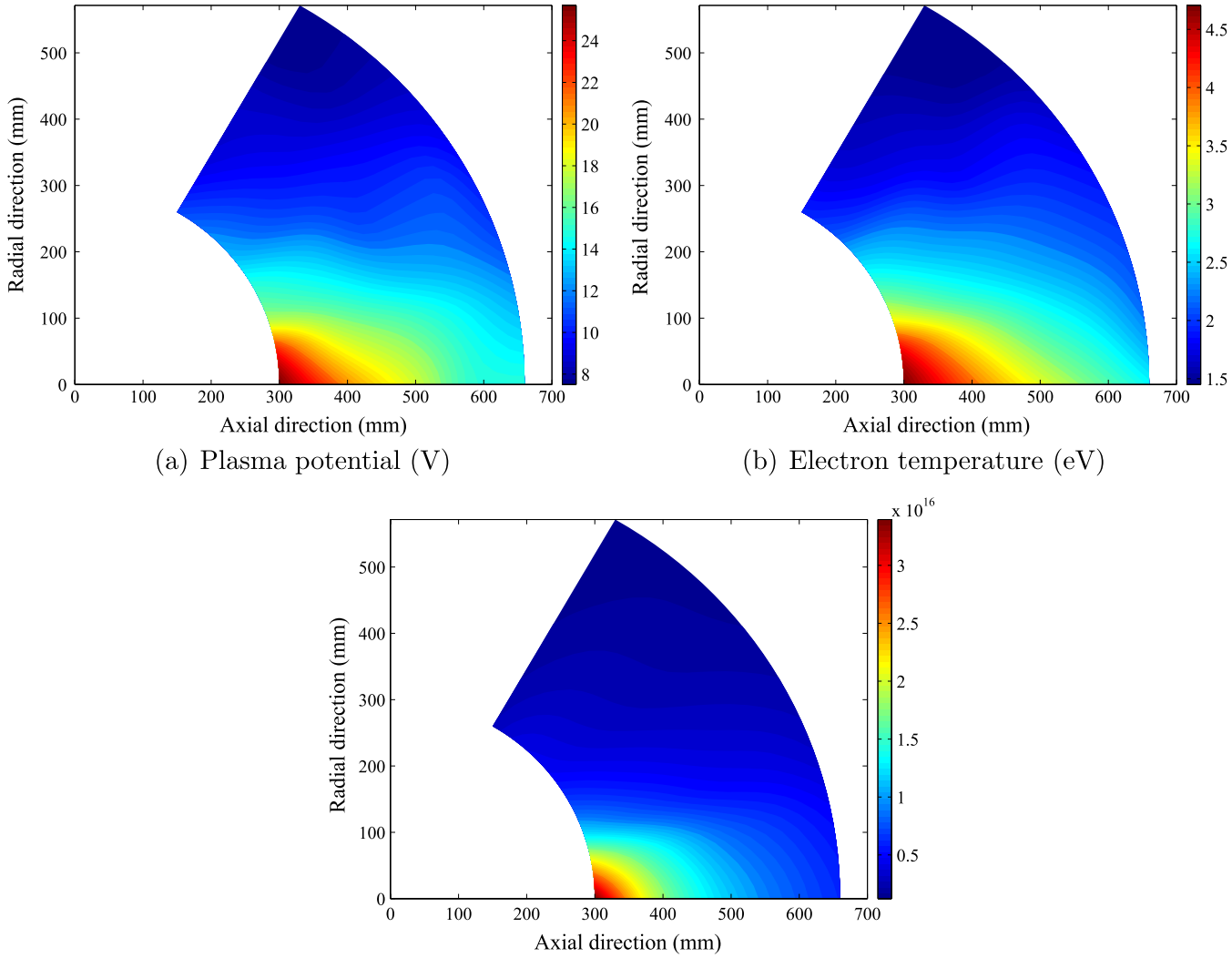

(a) Plasma potential (V)

(b) Electron temperature (eV)

(c) Electron number density (m^{-3})

Figure 4. Complete map of the far-field plume for $U_d = 300$ V, $\dot{m}_a = 4.0$ mg s^{-1}.

almost no difference for the three different discharge voltages. Figure 5(*c*) shows that the electron density n_e decreases with the angle θ. The electron density drops by a factor of 3 for $U_d = 300$ V, respectively by a factor of 2 for $U_d = 200$ V and by a factor of 1.5 for $U_d = 150$ V. Similar results for a SPT100 have been observed by Myers and Manzella [24].

3.3. Influence of the cathode mass flow rate

The far-field plume of the PPS100-ML with permanent magnets is mapped for three different cathode mass flow rates ($\dot{m}_c = 0.3$, 0.42 and 0.5 mg s^{-1}) at a discharge voltage of $U_d = 300$ V and a constant anode mass flow rate of $\dot{m}_a = 4.0$ mg s^{-1}. The results of the LP measurements are shown in figure 6 for two different distances from the thruster exit plane.

The cathode potential to ground is almost the same for $\dot{m}_c = 0.42$ and 0.5 mg s^{-1}, whereas it is significantly higher for $\dot{m}_c = 0.3$ mg s^{-1}, as can be seen from table 1. The mean discharge current and the current standard deviation are slightly lower for the lowest cathode mass flow rate, as shown in table 1.

Figure 6(*a*) shows the evolution of the plasma potential V_p. As can be seen, the values of V_p are almost the same for $\dot{m}_c = 0.42$ mg s^{-1} and $\dot{m}_c = 0.5$ mg s^{-1}. For $\dot{m}_c = 0.3$ mg s^{-1}, the values of V_p are higher than for the other two cathode mass flow rates. The electron temperature T_e is represented in figure 6(*b*). The highest values of T_e can be observed for $\dot{m}_c = 0.3$ mg s^{-1} and the lowest values of T_e are measured for $\dot{m}_c = 0.5$ mg s^{-1}. However, the difference for the two higher cathode mass flow rates is very small. As can be seen in figure 6(*c*), there is almost no difference for the electron density n_e for the three different cathode mass flow rates.

3.4. Influence of the magnetic field

The far-field plume of the standard version of the PPS100-ML (with coils) is mapped for three different currents through the coils at a discharge voltage $U_d = 200$ V, a constant anode mass flow rate $\dot{m}_a = 2.5$ mg s^{-1} as well as a constant cathode mass flow rate $\dot{m}_c = 0.42$ mg s^{-1}. The coil current was varied between 2.5 and 5.5 A which corresponds to a change in the maximum magnetic field strength from ≈100 to ≈200 G. The

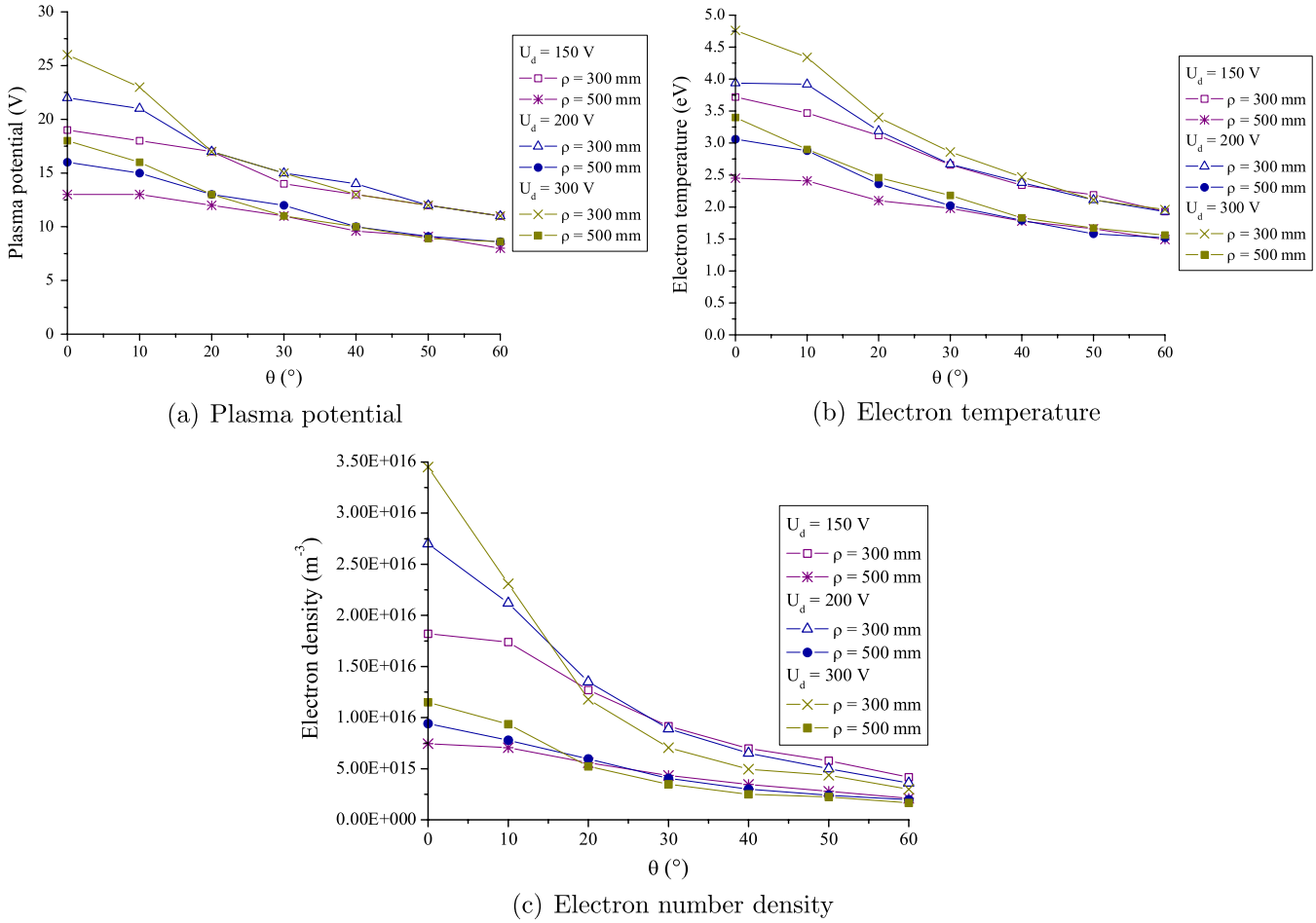

(a) Plasma potential (b) Electron temperature

(c) Electron number density

Figure 5. Influence of discharge voltage for $\dot{m}_a = 4.0\,\mathrm{mg\,s^{-1}}$ and $\dot{m}_c = 0.42\,\mathrm{mg\,s^{-1}}$.

Table 1. Mean discharge current, current standard deviation and cathode potential to ground for the different operating conditions of the PPS100-ML thruster.

Discharge voltage U_d (V)	Anode mass flow rate $\dot{m}_a$ (mg s^{-1})	Cathode mass flow rate $\dot{m}_c$ (mg s^{-1})	Coil current I_b (A)	Mean discharge current $\bar{I}_d$ (A)	Current standard deviation (A)	Cathode potential to ground (V)
150	4.0	0.42	—	3.46	0.23	−13.2
200	4.0	0.42	—	3.47	0.12	−14.4
300	4.0	0.42	—	3.65	0.35	−15.1
300	4.0	0.3	—	3.58	0.26	−19.2
300	4.0	0.5	—	3.67	0.34	−14.6
200	2.5	0.42	2.5	2.09	0.46	−12.2
200	2.5	0.42	4.5	1.9	0.17	−14.7
200	2.5	0.42	5.5	1.93	0.43	−14.5

optimized magnetic field topology of PPS100-ML is obtained for a coil current of 4.5 A. The evolution of V_p, T_e and n_e measured with an LP is depicted in figure 7 for two different distances from the thruster exit plane.

Table 1 shows that the cathode potential to ground is almost the same for $I_b = 4.5$ A and $I_b = 5.5$ A, whereas it is lower for $I_b = 2.5$ A. The mean discharge current is very similar for the two higher coil currents and slightly higher for the lowest coil current. The discharge current standard deviation is almost the same for $I_b = 2.5$ A and $I_b = 5.5$ A, but significantly lower for $I_b = 4.5$ A. This is in agreement with the fact the magnetic field topology is optimized for 4.5 A.

The plasma potential V_p is represented in figure 7(*a*); it decreases with the angle θ. The highest values for V_p can be observed for $I_b = 5.5$ A. At a distance of 500 mm from the thruster exit plane, the values of V_p are almost the same for $I_b = 4.5$ A and $I_b = 5.5$ A. The values for $I_b = 2.5$ A are significantly lower. The evolution of the electron temperature T_e is represented in figure 7(*b*). The values for $I_b = 4.5$ A and $I_b = 5.5$ A are very close, especially at a distance of 500 mm from the thruster exit. At 300 mm, T_e decreases up

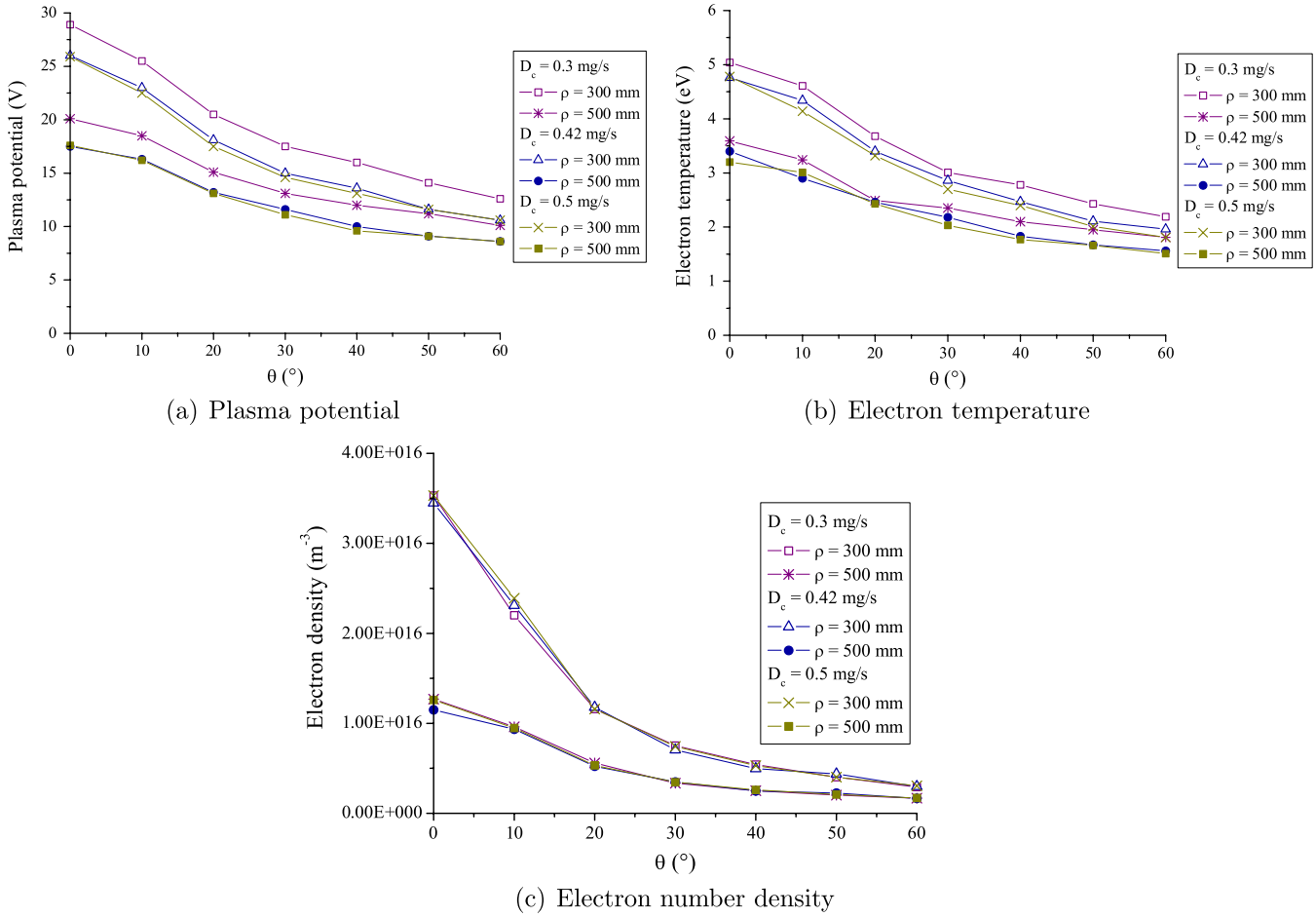

(a) Plasma potential (b) Electron temperature

(c) Electron number density

Figure 6. Influence of cathode mass flow rate for $U_d = 300\,V$, $\dot{m}_a = 4.0\,mg\,s^{-1}$.

to an angle of about 50° whereas for $\theta > 50°$, T_e is almost constant. At 500 mm, T_e decreases up to an angle of 20° and is almost constant for higher angles. The values for $I_b = 2.5\,A$ are significantly lower than for the other two coil currents I_b. For this configuration T_e decreases up to an angle of 40° and for higher angles T_e is almost constant. The evolution of the electron density n_e is represented in figure 7(*c*). The values for n_e are almost the same for the three different currents I_b, solely for $I_b = 2.5\,A$ n_e is slightly higher at $\theta = 0°$.

3.5. Comparison between LP and EP measurements

For all the different operating conditions, the plasma potential V_p was also measured using an EP. The plasma potential is assumed to be determined by the floating potential of the EP heated with a current of 4.5 A. An example for the plasma potential measured with an EP is given in figure 8. The PPS100-ML with permanent magnets was operated at discharge voltage of $U_d = 200\,V$ with an anode mass flow rate of $\dot{m}_a = 4.0\,mg\,s^{-1}$ and a cathode mass flow rate of $\dot{m}_c = 0.42\,mg\,s^{-1}$. Figure 9 shows the fractional difference D_{V_p} between the values measured with the LP and the EP, where $D_{V_p} = (V_{p,EP} - V_{p,LP})/V_{p,mean}$. As can be seen in the figure 9, the values of plasma potential obtained with an LP and an EP are in good agreement. The difference between the results obtained by both types of probes is on the order 5–10%, except for angles above 50° and more than 500 mm downstream the thruster exit plane. In this region the value of V_p is relatively small, which leads to a larger fractional difference. As can be seen in figure 9, in the region of higher electron temperature, i.e. close to the thruster axis, the EP gives slightly lower values for the plasma potential than the LP. In the region with a lower electron temperature, the plasma potential measured with the EP is higher than that measured with the LP. This qualitatively agrees with considerations described in section 2 and in [25]. Similar trends have also been observed by Marek *et al* in a low-temperature argon plasma [20].

The electron temperature can be determined from the EP measurements using the floating potential of the cold probe (ϕ_{fl}^{cold}) and the heated probe, which is assumed to be the plasma potential ($\phi_{fl}^{hot} = V_p$). In the far-field plume the value of the Debye length λ_d is between 90 and 180 μm, the probe radius is thus smaller than the Debye length. In this case the OML regime is valid and the electron temperature can be obtained by the following equation: $T_e = (V_p - \phi_{fl}^{cold})/5.24$ (in eV) [22]. A map of the electron temperature measured with an EP is displayed in figure 10 for the PPS100-ML with permanent magnets operated at a discharge voltage of $U_d = 200\,V$, with an anode mass flow rate of $\dot{m}_a = 4.0\,mg\,s^{-1}$ and a cathode mass flow rate of $\dot{m}_c = 0.42\,mg\,s^{-1}$. The fractional difference $D_{T_e} = (T_{e,EP} - T_{e,LP})/T_{e,mean}$ of the electron temperature measured with the LP and with the EP is shown in figure 11.

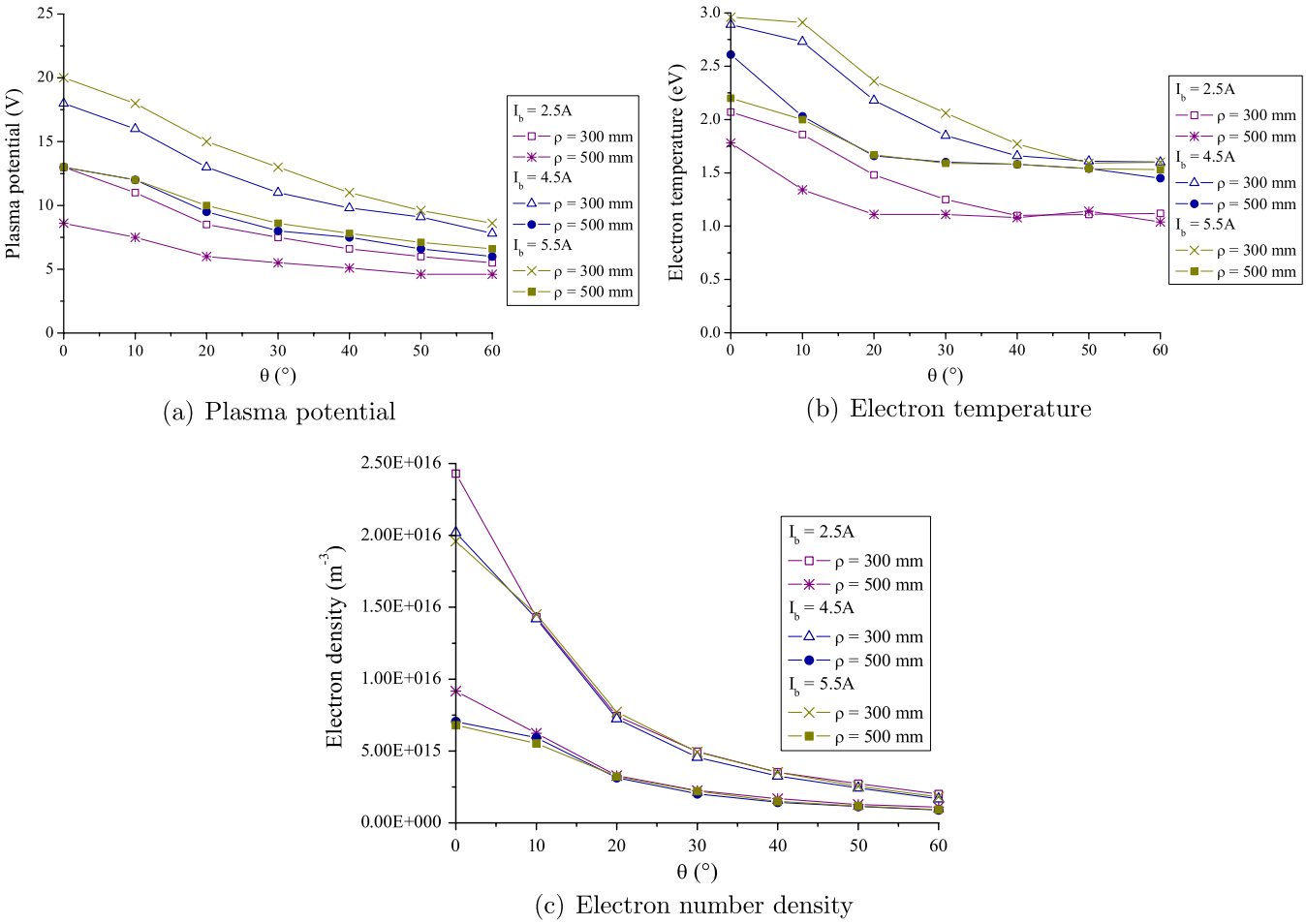

(a) Plasma potential

(b) Electron temperature

(c) Electron number density

Figure 7. Influence of coil current for $U_d = 200\,\text{V}$, $\dot{m}_a = 2.5\,\text{mg s}^{-1}$ and $\dot{m}_c = 0.42\,\text{mg s}^{-1}$.

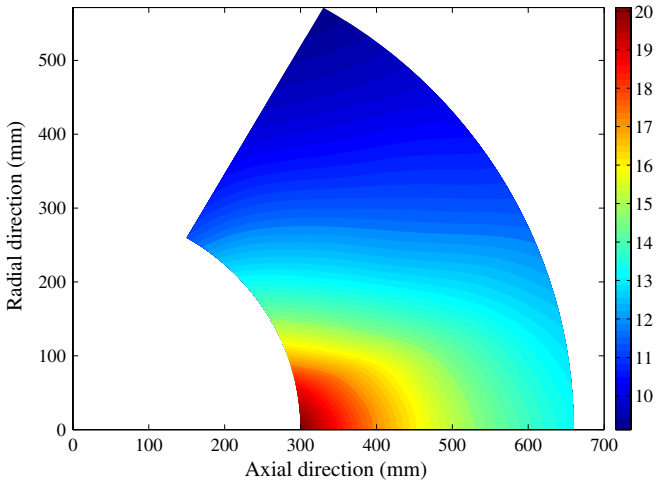

Figure 8. Plasma potential measured with an EP in the far-field plume of the PPS100-ML with permanent magnets at $U_d = 200\,\text{V}$ and $\dot{m}_a = 4.0\,\text{mg s}^{-1}$.

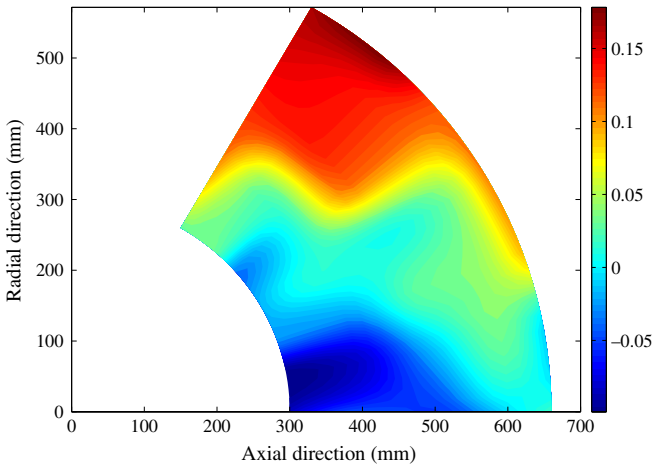

Figure 9. Fractional difference of plasma potential D_{V_p} measured with an EP and a LP for the PPS100-ML operating at $U_d = 200\,\text{V}$ and $\dot{m}_a = 4.0\,\text{mg s}^{-1}$.

As can be seen, the difference for the values obtained with the two different probes is 10–20% except for the near-axis area. The Debye length in the near-axis area is smaller than further off-axis. The OML-regime assumption is therefore less accurate in the near-axis area, which can explain the bigger difference between the two values. Figure 11 also shows that the electron temperature obtained by the EP measurements is underestimated in the near-axis area and overestimated in the off-axis area. This can be explained by the under-, respectively, overestimation of the plasma potential by the EP.

Although the absolute values of V_p and T_e are not exactly the same, both types of probes provide the same evolution of

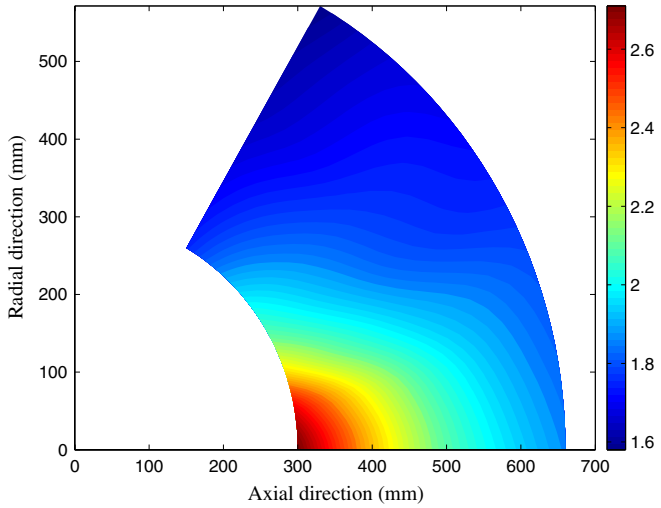

Figure 10. Electron temperature measured with an EP for the PPS100-ML operating at $U_d = 200$ V and $\dot{m}_a = 4.0$ mg s^{-1}.

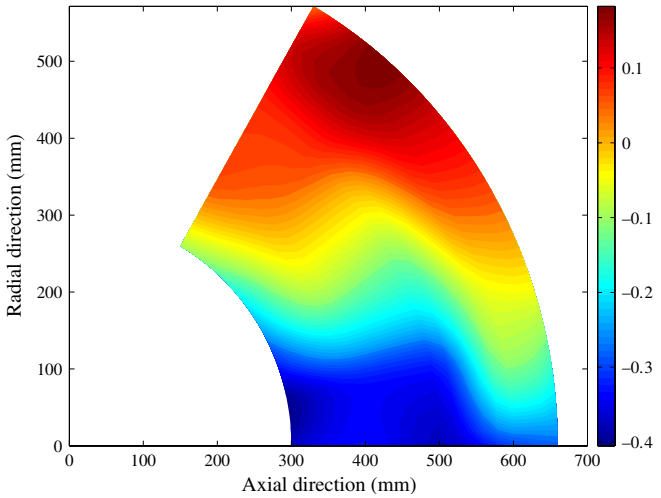

Figure 11. Fractional difference of electron temperature D_{T_e} measured with an EP and an LP for the PPS100-ML operating at $U_d = 200$ V and $\dot{m}_a = 4.0$ mg s^{-1}.

the plasma potential and electron temperature in the far-field and the difference between the values is relatively small. EPs are therefore a very interesting diagnostic tool as they provide a direct and instantaneous measurement of the plasma potential and the electron temperature. No voltage sweep or analysis of the current–voltage characteristics are needed as for an LP.

4. Conclusion

The far-field plume of the PPS100-ML Hall thruster was mapped using a Langmuir and an emissive probe. The plasma potential V_p, the electron temperature T_e as well as the electron number density n_e were measured between 300 and 660 mm downstream the thruster exit plane and between 0° and 60°. The influence of the discharge voltage, the cathode mass flow rate as well as the magnetic field strength on the plasma parameters was investigated. The results showed that the plume is an expanding plasma jet in a supersonic regime with cooling and recombination of electrons and ions [26]. The emissive probe and the Langmuir probe gave similar results for the plasma potential and electron temperature. Hence emissive probes can be used for the direct measurement of these two parameters.

The presented data set gives interesting insights into the physics of the downstream plasma of any crossed-field discharge; moreover, it is of great relevance for the validation and refinement of plume models. Yet, time-averaged measurements of the plasma parameters can only give a first estimate of the plasma plume properties. Time-resolved measurements are necessary to correctly measure the time-correlated plasma properties, as the plasma of crossed-field discharges and especially Hall effect thrusters is proved to be highly non-stationary.

Acknowledgments

This work is carried out in the frame of the CNRS/CNES/SNECMA/Universités joint research program GdR 3161 entitled '*Propulsion par plasma dans l'espace*'. MT and PK acknowledge the financial support by CNRS contract 48792.

References

[1] Zhurin V V, Kaufmann H R and Robinson R S 1999 *Plasma Sources Sci. Technol.* **8** R1–R2
[2] Annaratone B M, Escarguel A, Lefevre T, Rebont C, Claire N and Doveil F 2011 *Phys. Plasmas* **18** 032108
[3] Oudini N, Hagelaar G J M, Boeuf J P and Garrigues L 2011 *J. Appl. Phys.* **109** 073310
[4] Kaufmann H R, Robinson R S and Seddon R I 1987 *J. Vac. Sci. Technol.* A **5** 2081
[5] Rogister A L 2004 *Plasma Phys. Control. Fusion* **46** 573
[6] Hemsworth R S and Inoue T 2005 *IEEE Trans. Plasma Sci.* **33** 1799–813
[7] Kolev St, Lishev St, Shivarova A, Tarnev Kh and Wilhelm R 2007 *Plasma Phys. Control. Fusion* **49** 1349–69
[8] Frisbee R H 2003 *J. Propulsion Power* **19** 1129–54
[9] Goebel D M and Katz I 2008 *Fundamentals of Electric Propulsion* (Hoboken, NJ: Wiley)
[10] Koppel C R, Marchandise F, Prioul M, Estublier D and Darnon F 2005 *Proc. 41th Joint Propulsion Conf. (Tucson, Az)* AIAA 05-3671
[11] Hofer R R, Jankovsky R S and Gallimore A D 2006 *J. Propulsion Power* **22** 721–31
[12] Darnon F 2000 *Proc. 3rd Int. Conf. on Spacecraft Propulsion (Cannes, France)* ESA SP-465
[13] Mazouffre S, Lazurenko A, Lasgorceix P, Dudeck M, d'Escrivan S and Duchemin O 2007 *7th Int. Symp on Launcher Technologies (Barcelona, Spain)* Paper O-25
[14] Gascon N, Dudeck M and Barral S 2003 *Phys. Plasmas* **10** 4123–36
[15] Renaudin F, Cagan V, Guyot M, Cadiou A, Vial V and Dumazert P 2003 *Proc. 28th Int. Electric Propulsion Conf. (Toulouse, France)* IEPC 03-284
[16] Albarède L, Lago V, Lasgoceix P, Dudeck M, Bugrova A I and Malik K 2003 *Proc. 28th Int. Electric Propulsion Conf. (Toulouse, France)* IEPC 03-333
[17] Chung P M, Talbot L and Touryan K J 1975 *Electric Probes in Stationary and Flowing Plasmas: Theory and Application* (New York: Springer)
[18] Chen F F 1965 Electric probes *Plasma Diagnostic Techniques* ed R H Huddlestone and S L Leonard (New York: Academic) pp 113–200

[19] Ionita C *et al* 2011 *Contrib. Plasma Phys.* **51** 264–70
[20] Marek A, Jílek M, Picková I, Kudrna P, Tichý M, Schrittwieser R and Ionita C 2008 *Contrib. Plasma Phys.* **48** 491–6
[21] Smirnov A, Raitses Y and Fisch N J 2004 *J. Appl. Phys.* **95** 2283–92
[22] Raitses Y, Staack D, Smirnov A and Fisch N J 2005 *Phys. Plasmas* **12** 073507
[23] Smith A W and Cappelli M A 2009 *Phys. Plasmas* **16** 073504
[24] Myers R M and Manzella D H 1993 *Proc. 23rd Int. Electric Propulsion Conf. (Seattle, WA)* IEPC 93-096
[25] Takamura S, Ohno N, Ye M Y and Kuwabara T 2004 *Contrib. Plasma Phys.* **44** 126–137
[26] van de Sanden M C M, de Regt J M and Schram D C 1993 *Phys. Rev.* E **47** 2792–7